Modeling of the Thigh: a 3D deformable approach considering muscle interactions

Julien Stelletta, Raphaël Dumas, Yoann Lafon

▶ **To cite this version:**

Julien Stelletta, Raphaël Dumas, Yoann Lafon. Modeling of the Thigh: a 3D deformable approach considering muscle interactions. Biomechanics of Living Organs: Hyperelastic Constitutive Laws for Finite Element Modeling, pp.497-521, 2017. hal-01913274

HAL Id: hal-01913274
https://hal.science/hal-01913274

Submitted on 6 Nov 2018

HAL is a multi-disciplinary open access archive for the deposit and dissemination of scientific research documents, whether they are published or not. The documents may come from teaching and research institutions in France or abroad, or from public or private research centers.

L'archive ouverte pluridisciplinaire **HAL**, est destinée au dépôt et à la diffusion de documents scientifiques de niveau recherche, publiés ou non, émanant des établissements d'enseignement et de recherche français ou étrangers, des laboratoires publics ou privés.

Book Title: Biomechanics of Living Organs: Hyperelastic Constitutive Laws for Finite Element Modeling

Chapter: Part xx: Active organs

Title: Modeling of the Thigh: a 3D deformable approach considering muscle interactions

Authors: **Julien STELLETTA[a], Raphaël DUMAS[a], Yoann LAFON[a*]**

[a] Univ Lyon, Université Claude Bernard Lyon 1, IFSTTAR, UMR_T9406, LBMC, F69622, Lyon, France

Deadlines:

- End of March 2016: first draft submission
- End of June 2016: returns of the reviews
- End of August 2016: final papers
- October 2016: Proofs

Notes:

Authors involved in parts 2 and 3 (chapters 6 to 25) are asked to limit their text to 7 500 words (approximately 15 pages). There should be a maximum of 6/7 figures and/or tables per chapter with 2 to 3 figures that can be printed in color.

Abstracts (135 words). *"should be 100-150 words"*

A 3D deformable model of the thigh's musculoskeletal system has been developed. An adjucted multi-body rigid model was used to compute the bone kinematics and the muscle activation levels which drive a Finite Element model of the musculoskeletal system integrating contractile muscles. A thermomechanical beam model for muscle fibers was embedded in the passive muscle matrix meshed with hexahedrons with a hyperelastic quasi incompressible material law. Contacts between surrounding anatomical structures, transmitting radial forces, were modeled to investigate the effect of the interactions between muscles on the production of muscle forces. Two steps of the gait cycle were simulated. This study demonstrated that integrating such a deformable model could update the musculo-tendon forces traditionally computed from a multi-body rigid model that fails to take into consideration 3D fiber distribution as well as muscle tightening effect.

Keyword: thigh, 3D deformable contractile muscles, interactions between muscles, radial forces, multi-body rigid model, Hill-type model, gait

Words: 7353.

Modeling of the Thigh: a 3D deformable approach considering muscle interactions.

Introduction

Muscles contribute to the control of the bones kinematics and the joint stiffness, the stability during movements, and the propulsion for the movement task. The muscles transmit the force generated by the sarcomeres to bones through the myotendinous junction, but also transmit the force to surrounding anatomical structures by the connective tissue. Therefore, the relative position of muscles with respect to the surrounding anatomical structures could be of major importance on the muscle force production (Yucesoy, 2010). So dealing with muscles as isolated functional units producing force according to force-length/force-velocity relationships could lead to misestimate their actions. If the literature based on experiments and case-study models have largely investigate the myofascial force transmission as a shear loading (Purslow, 2010), Siebert et al. (2014) reported recently that the muscle force production could decrease due to a transverse compression: this opens up new understandings on the muscle force transmission to surrounding anatomical structures through radial loading. This appears as essential in the muscular architecture of the thigh. The musculoskeletal thigh system is made of the largest skeletal muscles of the whole body. The powerful thigh muscles, between the pelvis and the knee, contribute to the locomotion, the stability maintenance, and the support of the full body weight. Due to the large muscle loads applied, the hip joint, tibiofemoral and patellofemoral are ones of the most degenerative joints (Kim and James, 2012; Zhang and Jordan, 2010). If the lower limb is still one of the most investigated part in the body through musculoskeletal modeling, the complexity of muscular architecture of the thigh system often yielded to simplify its numerical representation.

Investigating musculoskeletal functions and disease requires a framework integrating a relevant soft tissue modeling as well as a physiological contractile ability within muscle models for relevant stress field and pressure estimation. However developing such a framework is still challenging, by gathering together mechanical, physiological and numerical issues under the constraints of allowing for future personalization (Fernandez et al., 2006). So the few authors investigating it chose a multi-body rigid model with reasonable computation cost for the computation of the boundary conditions (kinematics and musculo-tendon forces), to drive a deformable joint finite element model, most of the time, in quasi-static simulations (Adouni and Shirazi-Adl, 2013). However, driving a deformable

musculoskeletal model require to deal with large deformation of soft tissue, contact issues (implying heavy computational costs), and, in dynamic simulations, kinematically incompatible boundary conditions between the multi-body rigid model and the deformable musculoskeletal one, which limits the level of details of the latter. Moreover, modeling the whole musculoskeletal thigh system with a solid representation remains mainly based on a continuum mesh of the detailed anatomical structures, with passive muscle modeling as hyperelastic materials using first order Ogden law (Al-Dirini et al., 2016). In computer graphics applications (Lee, 2011), the simplest approach consists in a pure geometric deformation (i.e., without any material law) of the muscle surface according to the kinematics of bones, also called skinning (Dicko et al., 2013; Dong et al., 2002; Kohout et al., 2013; Murai et al., 2016). For more realistic approaches Li et al. (2013), Fan et al. (2014) and Sachdeva et al. (2015) proposed an Eulerian-on-Lagrangian (EOL) approach for skin, muscle and tendon models respectively. The Eulerian discretization allows efficient handling of large incompressible deformations, collision detection between many contacting muscles on a single and uniform grid per bone. However, the authors use a pure isotropic elastic material law without taking into account fibers, and reported numerical issues leading to unrealistic soft tissue deformations at the boundary of the grids. Authors from computer graphics were also ones of the firsts to drive complex musculoskeletal deformable models with bone kinematics and muscle activation levels computed from inverse dynamics analysis using an adjucted multi-body rigid model (Lee, 2011). The most tremendous framework was initiated by Teran et al. (2005). The authors constructed a model of the musculoskeletal system of the upper limb from the Visible Human dataset (with more than thirty muscles). To assure numerical convergence for a reduced computational cost, the authors developed a finite volume approach (which was a variation of the linear tetrahedral finite element formulation) corrected to deal with wrapped elements. Based on this work, Lee et al. (2009) increased the level of details of the musculoskeletal deformable model of the upper body, with 68 bones and 814 muscle actuators based on the linearized Hill-type law for the adjucted multi-body rigid model. Finally, Si et al. (2014) used this framework to simulate the whole human body swimming (with a model made of 103 rigid bones and 823 muscles). In all the three above mentioned studies, the muscle tissue was represented as a transverse isotropic material law: a Mooney-Rivlin rubber-like model for the passive part plus a deviatoric stretch in the along-fiber direction based on the activation level. The fiber direction inside each tetrahedron resulted from a B-spline interpolation. To avoid contact elements and speed up the simulation, a coarse tetrahedral mesh embedded the detailed musculoskeletal model. This embedding framework, called the “simulation mesh” by the authors, was initiated and theorized for general soft body deformation in Sifakis et al. (2007): the “simulation mesh” was an adaptively coarsen embedding tetrahedral mesh in which the detailed skin surface (triangulated mesh for rendering and collision handling), the fatty tissue, the muscles and the bones were

embedded. In the Teran/Lee approach, a network of spring constraints linked the deformable embedding mesh to the rigid articulated skeleton. Nodes of the embedding part close to the surface nodes of the embedded muscles were links for the muscle surface model, leading to a frictionless contact representation between muscles and avoiding the spurious separation of muscles. Another published framework proposed to use springs to model the interfaces between the biceps brachii muscle and its neighbors to conserve reasonable computation time over surface contact elements (Böl et al., 2011a, 2011b). The authors proposed a finite element model of the musculoskeletal upper arm to simulate isometric contraction in five arm positions. No bone kinematics was taken into account, the reconstruction of the geometry of the muscles being segmented from MRI at each position. The passive response of the muscle was based on a hyperelastic incompressible transversal isotropic constitutive law, with an along-fiber stretch contribution coming from the activation by electromechanical coupling. The interface spring stiffness were identified to fit experimental surface displacements on one point.

For applications related to medical engineering and research in biomechanics Fernandez et al. (2005) developed a framework based on cubic Hermite elements, to investigate the patella kinematics and pressure on it, driven by a flexion of the tibia, with deformable models of the quadriceps muscles (rectus femoris and the vastus group). The quadriceps were modeled without contacts between anatomical structures, the vastus muscles being fixed on the femur. The contact modeling was restricted to the interactions between the patella, the femur and the tendons from the patella. The muscle passive matrix was modelled with an orthotropic law with volume conservation. The fiber law was issued from cardiac activation tissue law: the fiber-based active contraction law guaranteed a local contraction field in the fiber field direction. However the activation level was arbitrary chosen only to assure the numerical stability. Behr (2006) proposed a solid model of the musculoskeletal of the lower limb for car crash applications. The hexahedron passive muscle mesh was associated to a viscoelastic anisotropic quasi-incompressible material law, with various elastic modulus depending on the fiber direction. Beams embedded in the solid mesh were chosen to model the fibers, and the activation level was represent as a thermal load. The contacts between muscles were represented, and the muscle activation was set through a thermomechanical coupling. However the lower limb was fixed in sitting posture and the activation levels were set arbitrarily. Blemker reported a model of the hip muscles and chiefs of the quadriceps (Blemker et al., 2005; Blemker and Delp, 2006). The authors proposed to model the muscle as a quasi-incompressible, fiber-reinforced composite with transversely isotropic material law to integer along-fiber shear strain, cross-fiber shear strain, and volume strain. The activation resulted in a modification of the along-fiber stretch contribution within the material law. If the authors proposed a framework to take into account a physiological complex

fiber field within the muscle material law, few muscles were finally modeled and the knee flexion was simulated using bone kinematics and a homogenous 20% activation level.

In this context, the present study presents an efficient approach for modelling the human thigh with 3D deformable contractile muscles driven by a set of muscle activations. The specific aim is to investigate the effect of the interaction between muscles, leading to radial loading, on the production of muscle forces. To succeed in modeling such a complex anatomical system, an adjucted multi-body rigid model was used to compute the bone kinematics and the muscle activation levels. These inputs drove a 3D deformable model of the musculoskeletal thigh system, with a robust contractile model based on a thermomechanical coupling: the fibers were modeled as beams with thermomechanical properties to represent the activation level as a variation of temperature, and then these fibers were associated to the passive matrix meshed with hexahedrons with a hyperelastic quasi incompressible law. Such an approach should guarantee to simulate a part of the gait cycle in a reasonable computational cost, taking into account the contacts between surrounding anatomical structures transmitting radial forces.

Background: anatomical and functional description of the organs

The osteoarticular system of the thigh is made of the femur, articulated with the pelvis through the hip joint and with the shank through the knee joint (tibiofemoral and patellofemoral joints).

Muscles of the thigh are clustered in three compartments, surrounding by the Fascia Lata (cf. Figure 2.1): the anterior compartment (including pectineus, sartorius, and the quadriceps with four chiefs: rectus femoris, vastus lateralis, medialis and intermedialis), the hamstring muscles of the posterior compartment (semimembranosus, semitendinosus, and the long and short heads of biceps femoris), the medial compartment muscles (adductor magnus, longus and brevis, and gracilis). At the hip level, the gluteal group is made of the gluteal muscles (minimus, medius, and maximus) and the Tensor Fascia Latae muscle.

[Insert Figure 2.1 here]

[Insert Figure 2.2 here]

As reported in figure 2.2, several muscles are involved in the thigh musculoskeletal system, leading to complex interactions during their contractions. Apart for the well-known agonist-antagonist synergies, mechanical connections through collagenous linkages also contribute to transmit forces intermuscularly through epimuscular myofascial force transmission (Yucesoy et al., 2010). Moreover,

the intramuscular extracellular matrix (made of the endomysium, perimysium and epimysium), but also the muscular septi, the aponeuroses and the joint capsules (depending of the fascia definition (Schleip et al., 2012)) are surrounding by the fascia. The fascia are any connective tissue linking all the anatomical structures (organ, muscles etc.) leading to a continuum throughout the human body (Findley and Shalwala, 2013). The connective tissue results in myofascial force transmission between adjacent muscles or group of muscles, and between muscular and non-muscular tissues. Fascia allowing the sliding between anatomical structures, the network of connective tissue should transmit shear loading between muscles. Fascia form an extensive network especially throughout the limb, with deep fascia defining a functional organization groups of muscles (i.e., the muscle compartments described above).

Material and Methods

1. Multi-body rigid modelling of the lower limb

The multi-body rigid model of the musculoskeletal system of the lower limb, used is adjunction to the deformable model, was developed previously (Moissenet et al., 2014). Five segments (pelvis, thigh, patella, shank and foot) were considered as rigid bodies, and articulated by four joints (ankle, tibiofemoral, patellofemoral and hip). The hip joint was modelled as spherical. The tibiofemoral joint was modelled as an equivalent mechanism made of two sphere-on-plane contacts for the medial and lateral compartments and three isometric ligaments (anterior cruciate, posterior cruciate and medial collateral ligaments). The patellofemoral joint was modelled as an equivalent mechanism made of a hinge joint between the patella and the femur and an isometric patellar tendon. The ankle joint was also considered as an equivalent mechanism, with a spherical talo-crural lateral contact and two isometric ligaments (between the tibia and the calcaneus, and between the fibula and the calcaneus).

The muscles were represented by 43 lines of actions (Delp et al., 1990), with via-points from the origins to the insertions to specify the muscle path. Some muscle geometries were divided into one to three parts to take into account extended insertion sites. The muscle lever arms were computed for each action line, yielded to a muscular redundancy. The multi-body rigid model of the musculoskeletal system of the lower limb is illustrated here after (cf. Figure 2.3).

[Insert Figure 2.3 here]

First, the segments positions, velocities and accelerations resulted from a typical multi-body kinematic optimization (under rigid body and joint-related kinematic constraints), to minimize the

squared distances between experimental and model-determined skin markers positions (Duprey et al., 2010). Second, the muscular redundancy problem was solved by inverse dynamics and static optimization, minimizing simultaneously the sum of the squared musculo-tendon forces contact forces, ligament forces and bones forces (Moissenet et al., 2014).

This model of the lower limb has been previously evaluated according to the « Grand Challenge Competition to predict in vivo knee loads » dataset, previously described in details (Fregly et al., 2012). A part of the second dataset was reused in the present study (Moissenet et al., 2014): the experimental data recorded for one subject (male, 83 year-old, 67 kg, 1.72 m) walking at a self-selected speed. Marker trajectories and ground reaction forces for one gait cycle were extracted from this dataset and used in this study. The multi-body rigid model was scaled to the subject anthropometry to fit the segments length and the bones kinematics and musculo-tendon forces were computed at every frame of the gait cycle. These information were used to drive the deformable model of the musculoskeletal system of the lower limb. For that, from the musculo-tendon forces and the musculo-tendon dynamics, the muscle activation levels were computed using a Hill-type model (Chèze et al., 2015).

2. Deformable modelling of the thigh

Geometry and Meshing

The detail geometry of the musculoskeletal system of the right thigh was issued from the manual segmentation of the Visible Human Project® (male) imagery dataset. The anatomical structures were manually segmented and cleaned before meshing. The five bones (pelvis, femur, patella, tibia, and fibula) were represented by the external wall of the cortical bones, to be considered as rigid bodies. The five ligaments (lateral [LL], medial collateral [ML], anterior cruciate [ACL], posterior cruciate [PCL]) and the patellar ligament [PL] were modeled with non-linear spring elements. The quadricipital tendon was meshed with tetrahedrons due to its thin shape.

The muscle matrix was meshed with hexahedral elements, oriented close to the line of action of each muscle. The solid meshing approach was based on a block template iteratively deformed to fit the muscle geometry, with a constraint on the quality of elements (scaled jacobian metrics upper than 0.4). The muscle fibers were modeled by a network of beam elements, in the principal orientation of each muscle (i.e. its line of action), and merged with the edge of hexahedrons (cf. Figure 2.4). The tetrahedral formulation was not considered, despite of meshing facility, to guaranty both a smooth field of deformation for a limited number of elements, and high quality elements supporting the

surface contacts for an effective transmission of loads even with large deformation. If recent complex methods could provide a full hexahedral mesh of the muscles, the deformation of a block to mesh muscles provided a simple space decomposition of the solid mesh into external layers and a deep volume with contraction capability, with a coherent numbering of nodes appropriate for the edge detection. In addition, the orientation of the solid mesh according to the line of action of muscles allowed to use beams for the fibers directly connected to the nodes of hexahedrons.

[Insert Figure 2.4 here]

17 muscles were considered to represent the musculoskeletal system of the thigh, with the three compartments of the thigh and the gluteal one for the hip. Quadrangle shell elements were extracted from the boundary of the solid part of the muscle to represent the aponeuroses of the muscle. For the muscle insertion and origin, the muscle mesh was attached to bones by using quasi-rigid elements, located at the anatomical insertions surfaces. The Tensor Fascia Latae muscle was not introduced in the model: after segmentation and meshing, the extremities of this muscle were far from the original ones in the image dataset to ensure quality of elements, leading to very long quasi-rigid elements modeling the insertion and, thus, non-physiologic lever arms. The minimal initial gap between anatomical structures was set to 5 mm. The whole deformable model of the lower limb consisted to 160.000 elements and 135.000 nodes (cf. Figure 2.5).

[Insert Figure 2.5 here]

Mechanical properties

The material properties of the ligaments and tendons were considered as elastic and isotropic, with Young's modulus of 0.15 MPa and a Poisson's ratio of 0.495. A hyperelastic law (Mooney-Rivlin, A = 8 MPa, B = 2 MPa, Poisson ration 0.490) for the quadriceps tendon. The passive and active properties of the muscles were represented, and a thermomechanical coupling approach was used to introduce the activation capability. A hyperelastic law (Mooney-Rivlin, A = 3 kPa, B = 0.75 kPa) was assigned to the quadrangle elements and to the hexahedral elements of the muscle matrix (Gras et al. 2011). A linear elastic thermo-mechanical law (E = 1 MPa, ALPHA = 0,01 $mm^3.K^{-1}$) was assigned to the beam network embedded into the solid mesh. The activation of the fibers was driven by the temperature imposed to the beams, yielding to a reduction in length as for the contraction task. A constant activation field was used for all the fibers of each muscle. For each muscle, the behavior was fitted on the Hill-type model (Zajac, 1988), by optimizing first the equivalent modulus of elasticity of the Mooney-Rivlin law for the passive behavior from the initial values above, and then the temperature

field for the global (i.e. passive and active) behavior for a given level of activation as reported by Stelletta et al. 2013 (cf. Figure 2.6). In the present study, only the active component was identified due to small elongations of the muscles for the gait cycle steps considered. The CC Hill-type model was chosen according to Siebert's recommendation between the two wildly used Hill-type models, to better represent the nonlinear contraction dynamics in musculoskeletal modeling (Siebert et al., 2008).

Boundary conditions and simulation

Two main steps of the gait cycle, the Heel Strike (HS) and the Loading Response (LR) steps, were simulated thanks to an explicit analysis with the LS-DYNA software (LSTC, Livermore, CA). The initial position of the lower limb model corresponded to the HS configuration as defined by the multi-body rigid model (i.e., multi-body kinematic optimization). First, the HS activation levels computed from the multi-body rigid model (i.e., static optimization) were applied to the fiber muscles of the deformable model according to a ramp function. From the previous configuration, the LR kinematics of the segments (corresponding to a 15° knee flexion) and the LR activation levels, both computed from the multi-body rigid model, were applied to the rigid bones and the fibers muscles of the deformable model, also through a ramp function. The kinematics and the activation levels were maintained to stabilize the mechanical behavior of the explicit integration scheme. A slight mass scaling was added to increase the time step from 10^{-6} to 10^{-5}s.

To investigate the effect of the interaction between muscles, two configurations were evaluated for each gait cycle step. The first configuration corresponded to the simulation based on the previous model; the second configuration consisted in adding contact surface elements between anatomical structures, to take into account the interaction between muscles and between muscles and bones. The perfect sliding contact model guarantee to transmit loads normal to the boundary only, according to the anatomical statement that "under the deep fascia, the muscles are free to slide because of their epimysium" (Stecco et al., 2011, 2008).

Post-processing

At the end of the Heel Strike (HS) and the Loading Response (LR) steps, the longitudinal force inside each thigh's muscle was computed. All the elements of the muscle mesh intersected by the cross section plane contributed to the longitudinal force: the net forces obtained in the beam, the solid and the shell elements intersected by the cross section were projected onto the normal of the plane. Thus, the addition of the projected total forces combine both the active (from the beam net forces) and passive contribution (from the solid and shell net forces). For comparison purpose, the musculo-

tendon force vectors computed from the multi-body rigid model were sum up when the muscle was modelled by multiple lines of actions.

Results

The multi-body rigid model of the musculoskeletal system of the lower limb was used to compute from experimental data the segment kinematics and the activation levels in all thigh muscles, for all the frames of the gait cycle. For both the Heel Strike (HS) and the Loading Response (LR) steps, some muscles presented a level of activation equal to zero. Using this information, the finite element simulations of the two gait cycle steps were successfully achieved in 10 minutes per configuration on a HP Z600 workstation (Quad Core Intel Xeon E5620 2.4Hz). Passive and active forces inside each muscle were computed from the finite element simulations. The total forces were reported in Table 2.6.

[Insert Table 2.6 here]

The two configurations of the deformable model, without and with contacts between anatomical entities, provided muscle forces always consistent with the multi-body rigid modelling of the lower limb, for the Heel Strike (HS) step. The mean [MAX] absolute difference on the total muscle forces was around 4.3N [20N] without contact, and 2.7N [10.3N] with contact. From a general view, there was no difference regarding the two configurations. Indeed for this gait cycle step, the bones were fixed and the only inputs were the muscle activation levels from the multi-body rigid model. So the contraction of the muscles was simulated isometric, without an evolution of the muscle cross section. In addition, in the absence of any variation of the muscle conformation due to the kinematics, the interaction between the muscles was limited: no geometric penetration was noted in the absence of contact element. The main differences with the muscle force patterns from the multi-body rigid model was due to a few modification of the muscle lever arms. As the origins and insertions were fixed, only the contraction tended to reduce the curvature of the muscles, resulting in a slight modification of the lines of actions and so of the produced muscle forces.

[Insert Figure 2.7 here]

For the Loading Response (LR) step, the two configurations of the deformable model yielded to muscle forces in the same order of magnitude than from the multi-body rigid modelling of the lower limb. The mean [MAX] absolute difference on the total muscle forces was slightly higher than for the HS step, around 13.0N [26.9N] without contact, and 17.5N [112.0N] with contact. For this step of the

gait cycle, the muscle deformable models presented large penetrations in the absence of contact (cf. Figure 2.7): the bone kinematics contributed to modify the interaction between structures in addition to a higher level of contraction.

Some muscles did not produced any forces according to the multi-body rigid model. In the deformable model, the solid passive part of the muscles had a material behavior yielding to a production of forces even for a negative strain field. However, the behavior of the muscle deformable model was optimized to fit the Hill-type model in traction, so the passive contribution was limited in compression. In addition, the muscles without activation being mainly in the medial and posterior compartments of the thigh, they moved away during the flexion of the knee. In the absence of the skin or any fascia clustering muscles in coherent groups, the contact status was not active for these muscles.

Discussion and Perspectives

This study reports a framework for modeling the musculoskeletal system of the human thigh, combining an adjucted multi-body rigid model to compute bone kinematics and muscle activation levels from experiments, and a driven solid deformable muscle models with contractile ability. The specific aim was to investigate the effect of the interaction between muscles, leading to radial loading, on the production of muscle forces. The kinematics and muscle activation levels were computed from experimental data by using a model of the lower limb which was previously validated against in vivo joint contact forces (Moissenet et al., 2014). The contractile ability in the deformable solid musculoskeletal system was modelled by a thermomechanical coupling on muscle fiber beams embedded in the muscle passive solid hexahedral meshes. The global behavior of each of the 17 muscles was fitted to represent a Hill-type model. Interactions and so radial loading between anatomical structures was considered through surface-to-surface contact elements.

Modelling choices

Several authors modelled a set of deformable muscles with a hyperelastic quasi-incompressible law model for the passive part (often used for rubbers), with a contribution resulting from a deviatoric stretch in the along-fiber direction based on the activation level (Blemker and Delp, 2006; Böl et al., 2011b; Lee et al., 2009; Sifakis, 2007; Si et al., 2014; Teran et al., 2005). However, the Teran/Lee approach did not include neither any anisotropic shear behavior relative to the fiber axis nor a realistic muscle constitutive model: the activation parameter was limited to produce a bulk length

from the contraction along the muscle fiber directions. As pointed by (Sifakis, 2007), this simplified approach had to be improved to investigate a more physiological behavior of the muscles. This was proposed by Blemker et al. (2005): the authors reported a muscle material model integrating an anisotropic material law with along-fiber stretch, with volume control and cross-fiber shear. This full material model was reused later, for example by Sanchez et al. (2014). For the fiber field, Blemker et al. (Blemker and Delp, 2006, 2005) deformed a complex template from a generic cube to the muscle surface (as Webb et al. (2014) and Berranen et al. (2014) later). Defining the fibers' force contribution as a contribution to the total strain energy function provided a simple solution to take into account the fiber field within the muscle matrix. Conversely, our choice was to dissociate the active and passive contributions of the fiber and the matrix. Few authors reported such a discrete approach to model the muscle through a truss/beam network embedded in a passive hexahedron mesh. To our knowledge, Behr (2004) was the first published work reporting such a reinforced approach. Its numerical simplicity and so robustness allowed to model 16 muscles for the lower limb, under one activation level for on position of the limb. Böl and Reese (2008) improved this approach in initiating the Sartorius muscle mechanical response (i.e. the fiber truss stretch) by motoneuron discharges, to vary the muscle force in modulating the rate of impulses driving the muscle fibers. Note that these authors decomposed the hexahedral elements in tetrahedral ones. Roux et al. (2016) reported a reinforced discrete formulation evaluated on a passive generic muscle, even if such an approach should not be able to take into account shear loading within the muscle tissue. Using an activation being computed from an adjusted multi-body rigid model to drive a deformable muscle make sense only if the deformable muscle provide a global behavior compatible with a Hill-type model (as we made by optimization). Using a 1D Hill-type element as fiber elements within a solid matrix (Hedenstierna et al., 2009), instead of a thermomechanical relationship, would not have prevented to make such an optimization process in order to ensure a consistent global muscle behavior. In addition, the initial length being different for each beam modeling the fiber field, this 1D Hill-type element approach required to define one material law per fiber, which is quite tedious (Howley, 2014). Berranen et al. (2014, 2012) proposed to embed Hill-type contractile 1D elements within the tetrahedral mesh of the matrix. They reused a force function for their contractile element previously reported by Böl and Reese (2008): they introduced the maximum isometric force of the whole muscle and the fiber density in the Hill-type elements to assure a coherence with the classical Hill-type model as used in multi-body rigid models, even for bipennate or pennate organization, without additional optimization. The link between the fibers and the passive tissue was obtained by considering the fiber forces due to contraction as external forces applied to the embedding passive muscle mesh. Another solution would have been to use constraint equations to link non-coincident nodes between fibers and solid elements. However, this could lead to numerical issues in large

deformation. So Berranen solved the well-known numerical issues in large rotation by filtering out local rotational modes, as for co-rotational FEM. Finally some authors provided more realistic approaches to model the muscle, until the integration of cellular models; but these formulations, only investigated on models representing one isolated muscle, are recognized as presenting too high computational complexity for an integration in a complete musculoskeletal model (Kockova and Cimrman, 2009; Röhrle et al., 2012; Wisdom et al., 2015; Zöllner et al., 2012).

We choose to model the muscle as an isotropic passive mesh reinforced by fiber beams. Hodgson et al. (2012) reported, by using a 2D numerical model, that the material properties of the passive muscle matrix could significantly influence the deformation field within a contracting muscle as well as the force produced, despite of various pennation angles. Thus they suggested to use an anisotropic passive matrix. As reported by Böl et al. (2014) on porcine biceps femoris muscles, the passive muscle tissue with the fibers embedded in the extracellular matrix presents an anisotropic response perpendicularly to the fiber direction, limiting the relevance of decomposing the passive muscle in an isotropic part relating to the extracellular matrix and an anisotropic part related to fibers.

Interactions between muscles

The results of the present study demonstrate an effect of taking into account the interactions between anatomical structures on the forces produced by muscle forces computed from classical multi-body rigid modelling (i.e., inverse dynamics and static optimization) based on experimental data. Both with and without contacts between anatomical entities, the deformable model provided muscle forces consistent with the multi-body rigid models of the lower limb. In detail, for both the two gait cycle steps, some muscles provided exactly the same total forces without and with contacts, while some muscles produced slightly more forces when introducing contacts (the deepest vastus medialis and the superficial Sartorius in HS, the deeper semimembranosus and the superficial gluteal medius in LR). Basically, this study pointed out the limitations of multi-body rigid modelling and the pertinence of finite element modelling to investigate the biomechanics of muscle contraction. The limitations of multi-body rigid models are well-known: muscles are represented by their lines of action between origins and insertions, sometimes with intermediate via-points (more rarely with warping surfaces) for keeping consistent moment arms (especially for the muscles crossing the hip). Such a simplified approach assumes mass-less muscle, the segment mass being embedded to a fixed point of the bone. The physiological 3D fiber distribution as well as muscle tightening effects are ignored. The inability to represent the transmission of radial forces is less often stated but of paramount importance. Several authors reported a force transmission effect as a “transverse

loading" or a "lateral force transmission", which consists in the transmission of forces by shear stresses in the intramuscular connective tissue or in the extracellular matrix of skeletal muscle (Purslow, 2010). This kind of force transmission corresponds to a tangential loading with respect to the muscle surface. Others loadings are the axial loading (i.e. in the direction perpendicular to the cross section plane of the slender muscle structure, also called "longitudinal force" by some authors) and the radial loading (i.e. normal to the surface of the muscle, the one currently investigated in this study). Authors pointed, mainly on animal models (Huijing et al., 1998; Maas et al., 2001; Yucesoy et al., 2010), that the connecting tissue between muscles influenced the longitudinal muscle force, due to myofascial force transmission from surrounding muscles (Monti et al., 1999). Within isolated intact mammalian muscles, Ramaswamy et al. (2011) reported that the axial and the tangential force transmission were equal in rats and mice, for different force levels. More recently Zhang and Gao (2014) concluded on the impaired tangential force transmission in old rats.

The effect of the *in vivo* radial loading (i.e. due to muscle compression by surrounding muscles, connecting tissue, and bones) on the muscle force have not been investigated to our knowledge. By considering any muscle almost as isochoric (the muscle contains about 80% of water (Van Loocke et al., 2008)), the surrounding muscles should radially load any deeper muscle, leading to an increase of the muscle force because the internal muscle pressure is related to the muscle force under isometric conditions (Davis et al., 2003; Winters et al., 2009). But Siebert et al. (2016) reported that increasing the internal pressure lead to decrease the longitudinal muscle force. Thus, in our study the deepest gluteus minimus yielded to a total force drastically lower by taking into account contacts between muscles, at LR only. The gluteus minimus was caught between the pelvis and the other gluteal muscles, displaying high contraction. Siebert et al. (2014) reported, from isometric experiments on rat, that increasing the transversal (i.e. radial) muscle loading resulted in a decrease in the muscle force. Van Loocke et al. (2006) pointed that only a transversely isotropic hyperelastic model was able to capture the passive muscle in compression; and Van Loocke et al. (2008) reported a significant stiffening effect with compression rate and fiber orientation for passive muscle in compression (approximately 50% of total stress at 0.5 %strain.s^{-1}).

Limitations

Fiber field representation

The fibers were aligned with the curved direction between the origin and insertion of each muscle, to stay as close as possible to the adjucted multi-body rigid model with Hill-type muscle model. To improve our model, the physiological 3D fiber field could be extracted from imaging (Kwah et al., 2013; Levin et al., 2011; Schenk et al., 2013; Zhukov and Barr, 2003) with a preference for DTI over

ultrasound (Bolsterlee et al., 2015; Damon et al., 2011) even with 3D position tracker system, based on a template fitted to the muscle geometry either from anatomical observation (Blemker and Delp, 2005) or from digitized *in vitro* muscle specimens (Lee et al., 2015; Sanchez et al., 2014), or computed from theoretical approaches (Choi et al., 2015; Inouye et al., 2015; Wong and Kuhl, 2014). If more physiological curvature and length of the fascicles could explain non uniform strain inside the muscle volume especially around the aponeurosis (Azizi and Deslauriers, 2014; Blemker et al., 2005) with greater intramuscular pressure in deeper regions of muscles (Rana et al., 2013), the total force produce by the muscle should stay unchanged. Moreover, our aim was not to compute the strain field within muscles (which is also influenced by the chosen activation function (Stelletta et al., 2013) or the aponeurosis morphology (Rehorn and Blemker, 2010)), but the total force produced by the muscles. In addition to the 3D architecture, Siebert et al. (2015) pointed also the necessity to use specific force-length and force-velocity relationships according to the considered muscles. In our quasi-static approach, thermomechanical parameters were optimized to identify a behavior coherent with the normalized force-length relationship: the global behavior of each muscle was in agreement with the Hill-type model classically used in multi-body rigid model, with distinct force-length relationship considered for all the thigh muscles (Delp et al., 1990; Klein Horsman et al., 2007).

Aponeuroses, Fascia and tendon representation

Neither the external fascia nor the skin are taken into account in our model, so the muscle packaging effect is *a priori* insufficiently represented. Turrina et al. (2013) reported that “endomysium, perimysium, epimysium and deep fasciae have not just a role of containment, (…), but are fundamental elements for the transmission of muscular force”. The deep fascia define compartments separating functional groups of muscles, which are generally named according to the actions of their contained muscles: flexors, extensors, adductors, etc. (Benjamin, 2009). Two studies (Eng et al., 2014; Pancheri et al., 2014) pointed that the biaxial material properties of Fascia Lata could be related to the ability of the longitudinal Fascia Lata to transmit force, while allowing larger strains in the transverse direction to allow expansion in case of muscle contraction. This comment regarding the biaxial material properties is the same for the aponeuroses, which exhibit an anisotropic 3D structure, with a transverse stiffness four times lower than the longitudinal one (Azizi and Roberts, 2009). In our model, the aponeuroses of the muscles were simplified to a shell approach with an isotropic nonlinear material law. A more realistic material model could contribute to homogeneous fascicle length change during contraction (Muramatsu et al., 2002). In addition, our muscle geometry (and so the aponeurosis morphology) was simplified during the meshing process to guarantee a high element quality: Rehorn and Blemker (2010) and Fiorentino and Blemker (2014) reported that a simplified aponeurosis model could drastically decrease the along-fiber stretch across all the muscle

tissue, the peak of the along-fiber stretch within the muscle being related to geometry of the aponeuroses.

In our model, the tendons were represented as an elastic beam network with a global behavior stiffer than muscle tissue converging towards a stiffness matrix (Calvo et al., 2010): introducing the tendon material law should not pose additional complexity, the nonlinear stress–strain relationship being similar to aponeuroses (Scott and Loeb, 1995).

History of activation and muscle force enhancement

We considered the muscle activation for two steps in the gait cycle, by simulating the Heel Strike (HS) step followed by the Loading Response (LR) one. Simulations were performed with an explicit scheme but represented quasi-static conditions which are consistent with the activation levels computed from the adjucted multi-body rigid model. In the literature, a muscle force enhancement (Herzog et al., 2008) has been noted both from in vitro experiments and from in vivo ones on large human muscles under physiological conditions (Abbott and Aubert, 1952; Hahn et al., 2007; Seiberl et al., 2010). Herzog (2004) pointed that the force history dependence could raise up to 50% of the corresponding isometric reference force, through the active and the passive structures (Herzog and Leonard, 2005). However, for example the muscle force enhancement is not related to a history-based variation of fascicle lengths and pennation angles (Tilp et al., 2011). So modeling the force history dependence is difficult due to various hypothesis (mainly out of mechanical parameters) to explain this phenomenon (Campbell and Campbell, 2011), leading to more complex continuum-mechanical model of skeletal muscle including actin–myosin interactions and actin–titin interactions (Heidlauf et al., 2016). Due to the quasi-static approach, no history dependence of the forces produced by the muscles in isometric state was taken into account in the model, as for the Hill-type model. So the history of the boundary conditions applied to the model was the simulation of the muscle contraction, followed by the introducing the bone kinematics to facilitate the numerical convergence.

Conclusion and perspectives

In our approach, the skeletal muscles were modelled as a fiber reinforced continuum, allowing the force transmission between fibers through the passive matrix's solid elements, particularly by shear loading. Regarding the force transmission between muscles, only the radial loading was considered in this study by using sliding contacts between anatomical structures. The tangential loading between structures was also not possible because the connecting tissue was not represented. For a given activation level, the muscle stiffness (activated or not) could increase due to the radial forces

transmitted from the surrounding muscles. The present results could extend the concept of "continuity of tissues" between muscles to the radial loading.

No definitive conclusion regarding the quantification of the interaction effects on the production of muscle forces from given activation levels would be taken from these results. For a given activation level, the deep muscles could produce higher forces by taking into account the ability to transfer loads between muscles, their whole surfaces being loaded. Moreover, the presence of contacts on the superficial muscles modified their lines of action during the movement, and therefore altered their forces. The main conclusion is that integrating a deformable model with interactions between anatomical structures could correct the musculo-tendon forces traditionally computed from a multi-body rigid model. As a matter of fact, the force transmission limited only to the tendons is a clear limitation of multi-body rigid modelling that is rarely stated in the literature. An extended study should be pursue on others steps of the gait cycle, even if the two chosen ones were so because of their complementarity in terms of boundary conditions. The effect of the interactions between muscles could depend on the bone kinematics, the activation levels of surrounding muscles, the spatial curvature of the fiber network, and the initial conformation of the muscles.

In the present study, the fasciae, the skin and the connecting tissue were not modeled. An initial gap between all anatomical structures was assessed to guaranty non initial penetration which compromises any simulation. Only the surface muscles were able to radially interact with deep muscles if their lines of action changed, either because of their contraction (if they were activated) or their traction (resulting from the bone kinematics, here the knee flexion). Grouping muscles in compartment through fasciae should be assessed in the future, to keep the coherence of anatomical structures and thus render a possible muscle packaging effect. However, such an approach induces to mesh the muscles in a different way, to drastically respect the initial geometry and guarantee no initial penetration. Presently, the initial geometry of the muscle were modified to guarantee high quality hexahedron elements. Further Investigation on meshing methods should be required to preserve the surfaces of muscles, and modeling the tendons as deformable structures, which could modify the global stiffness of the muscle-tendon complex and thus the produced muscle force. In addition, the next meshing step to improve the modeling of the muscles should be focused on dissociate the active truss/fibers from the solid passive muscle mesh, to consider a more realistic fiber field embedded in the muscle matrix mesh as in concrete modeling.

The final improvement step should be focused on evaluating the coherence of the model. Regarding the modeling of each muscle, one could find the inspiration in Sturmat et al. (2012) and then Böl et al. (2013) who reported presently one of the most comprehensive approaches to quantify the muscle

behavior on animal models. Regarding groups of muscles in their surrounding structures, few quantitative information are easily measurable from in vivo experiments. Ultrasound elastography for studying in vivo muscle stiffness appears presently as the state-of-the-art non-invasive (and simplest) method, with a high potential to investigate muscle properties, despite an underlined theory built on strong hypothesis (Brandenburg et al., 2014; Eby et al., 2013). The strain field within human muscles during in vivo contraction is also measurable using magnetic resonance imaging (Huijing et al., 2011), cine PC MRI (Pappas et al., 2002; Sinha et al., 2015; Zhong et al., 2008) or by combining diffusion and strain tensor MRI (Englund et al., 2011). The advantage of finite element modelling, giving access to strain in the muscle tissue, appears evident for such validations. Moreover, the deformable model of the thigh was driven by the bone kinematics and activation levels corresponding to experimental dataset taken from the « Grand Challenge Competition to predict in vivo knee loads ». This experimental dataset include the tibiofemoral contact forces measured by an instrumented prosthesis, usable to validate the present deformable model as it was done for the multi-body rigid model. For this purpose, the boundary conditions in terms of bone kinematics shall be further released until joint equilibrium is obtained, which is often considered as a great numerical challenge.

Acknowledgements

Funding for this work was provided by the Agence Nationale pour la Recherche, ANR-10-JCJC-0911, MIME Project. This work was performed within the framework of the LABEX PRIMES (ANR-11-LABX-0063) of Université de Lyon, within the program "Investissements d'Avenir" (ANR-11-IDEX-0007) operated by the French National Research Agency (ANR).

Conflict of interest statement

There are no conflict of interest for any of the authors.

Bibliography

Abbott, B.C., Aubert, X.M., 1952. The force exerted by active striated muscle during and after change of length. J. Physiol. 117, 77–86.

Adouni, M., Shirazi-Adl, A., 2013. Consideration of equilibrium equations at the hip joint alongside those at the knee and ankle joints has mixed effects on knee joint response during gait. J. Biomech. 46, 619–624. doi:10.1016/j.jbiomech.2012.09.035

Al-Dirini, R.M.A., Reed, M.P., Hu, J., Thewlis, D., 2016. Development and Validation of a High Anatomical Fidelity FE Model for the Buttock and Thigh of a Seated Individual. Ann. Biomed. Eng. 1–12. doi:10.1007/s10439-016-1560-3

Azizi, E., Deslauriers, A.R., 2014. Regional heterogeneity in muscle fiber strain: the role of fiber architecture. Front. Physiol. 5, 303. doi:10.3389/fphys.2014.00303

Azizi, E., Roberts, T.J., 2009. Biaxial strain and variable stiffness in aponeuroses: Biaxial strain in aponeuroses. J. Physiol. 587, 4309–4318. doi:10.1113/jphysiol.2009.173690

Behr, M., 2004. Description et modélisation du comportement musculaire des membres pelviens. Université de Marseille.

Behr, M., Arnoux, P.-J., Serre, T., Thollon, L., Brunet, C., 2006. Tonic finite element model of the lower limb. J. Biomech. Eng. 128, 223–228.

Benjamin, M., 2009. The fascia of the limbs and back - a review. J. Anat. 214, 1–18. doi:10.1111/j.1469-7580.2008.01011.x

Berranen, Y., Hayashibe, M., Gilles, B., Guiraud, D., 2012. 3D volumetric muscle modeling for real-time deformation analysis with FEM, in: Engineering in Medicine and Biology Society (EMBC), 2012 Annual International Conference of the IEEE. IEEE, pp. 4863–4866.

Berranen, Y., Hayashibe, M., Guiraud, D., Gilles, B., 2014. Real-time Muscle Deformation via Decoupled Modeling of Solid and Muscle Fiber Mechanics, in: Medical Image Computing and Computer-Assisted Intervention–MICCAI 2014. Springer, pp. 65–72.

Blemker, S.S., Delp, S.L., 2006. Rectus femoris and vastus intermedius fiber excursions predicted by three-dimensional muscle models. J. Biomech. 39, 1383–1391. doi:10.1016/j.jbiomech.2005.04.012

Blemker, S.S., Delp, S.L., 2005. Three-Dimensional Representation of Complex Muscle Architectures and Geometries. Ann. Biomed. Eng. 33, 661–673. doi:10.1007/s10439-005-1433-7

Blemker, S.S., Pinsky, P.M., Delp, S.L., 2005. A 3D model of muscle reveals the causes of nonuniform strains in the biceps brachii. J. Biomech. 38, 657–665. doi:10.1016/j.jbiomech.2004.04.009

Böl, M., Ehret, A.E., Leichsenring, K., Weichert, C., Kruse, R., 2014. On the anisotropy of skeletal muscle tissue under compression. Acta Biomater. 10, 3225–3234. doi:10.1016/j.actbio.2014.03.003

Böl, M., Leichsenring, K., Weichert, C., Sturmat, M., Schenk, P., Blickhan, R., Siebert, T., 2013. Three-dimensional surface geometries of the rabbit soleus muscle during contraction: input for biomechanical modelling and its validation. Biomech. Model. Mechanobiol. 12, 1205–1220. doi:10.1007/s10237-013-0476-1

Böl, M., Reese, S., 2008. Micromechanical modelling of skeletal muscles based on the finite element method. Comput. Methods Biomech. Biomed. Engin. 11, 489–504. doi:10.1080/10255840701771750

Böl, M., Sturmat, M., Weichert, C., Kober, C., 2011a. A new approach for the validation of skeletal muscle modelling using MRI data. Comput. Mech. 47, 591–601. doi:10.1007/s00466-010-0567-0

Böl, M., Weikert, R., Weichert, C., 2011b. A coupled electromechanical model for the excitation-dependent contraction of skeletal muscle. J. Mech. Behav. Biomed. Mater. 4, 1299–1310. doi:10.1016/j.jmbbm.2011.04.017

Bolsterlee, B., Veeger, H.E.J. (DirkJan), van der Helm, F.C.T., Gandevia, S.C., Herbert, R.D., 2015. Comparison of measurements of medial gastrocnemius architectural parameters from ultrasound and diffusion tensor images. J. Biomech. 48, 1133–1140. doi:10.1016/j.jbiomech.2015.01.012

Brandenburg, J.E., Eby, S.F., Song, P., Zhao, H., Brault, J.S., Chen, S., An, K.-N., 2014. Ultrasound Elastography: The New Frontier in Direct Measurement of Muscle Stiffness. Arch. Phys. Med. Rehabil. 95, 2207–2219. doi:10.1016/j.apmr.2014.07.007

Calvo, B., Ramírez, A., Alonso, A., Grasa, J., Soteras, F., Osta, R., Muñoz, M.J., 2010. Passive nonlinear elastic behaviour of skeletal muscle: Experimental results and model formulation. J. Biomech. 43, 318–325. doi:10.1016/j.jbiomech.2009.08.032

Campbell, S.G., Campbell, K.S., 2011. Mechanisms of residual force enhancement in skeletal muscle: insights from experiments and mathematical models. Biophys. Rev. 3, 199–207. doi:10.1007/s12551-011-0059-2

Chèze, L., Moissenet, F., Dumas, R., 2015. State of the art and current limits of musculo-skeletal models for clinical applications. Mov. Sport Sci. - Sci. Mot. 7–17. doi:10.1051/sm/2012026

Choi, H.F., Chincisan, A., Magnenat-Thalmann, N., 2015. A Collective Approach for Reconstructing 3D Fiber Arrangements in Virtual Musculoskeletal Soft Tissue Models, in: Doyle, B., Miller, K., Wittek, A., Nielsen, P.M.F. (Eds.), Computational Biomechanics for Medicine. Springer International Publishing, Cham, pp. 117–128.

Damon, B.M., Buck, A.K., Ding, Z., 2011. Diffusion-tensor MRI-based skeletal muscle fiber tracking. Imaging Med. 3, 675–687. doi:10.2217/iim.11.60

Davis, J., Kaufman, K.R., Lieber, R.L., 2003. Correlation between active and passive isometric force and intramuscular pressure in the isolated rabbit tibialis anterior muscle. J. Biomech. 36, 505–512. doi:10.1016/S0021-9290(02)00430-X

Delp, S.L., Loan, J.P., Hoy, M.G., Zajac, F.E., Topp, E.L., Rosen, J.M., 1990. An interactive graphics-based model of the lower extremity to study orthopaedic surgical procedures. IEEE Trans. Biomed. Eng. 37, 757–767. doi:10.1109/10.102791

Dicko, A., Gilles, B., Faure, F., Palombi, O., 2013. From generic to specific musculoskeletal simulations using an ontology-based modeling pipeline, in: Intelligent Computer Graphics 2012. Springer, pp. 227–242.

Dong, F., Clapworthy, G.J., Krokos, M.A., Yao, J., 2002. An anatomy-based approach to human muscle modeling and deformation. Vis. Comput. Graph. IEEE Trans. On 8, 154–170.

Duprey, S., Cheze, L., Dumas, R., 2010. Influence of joint constraints on lower limb kinematics estimation from skin markers using global optimization. J. Biomech. 43, 2858–2862. doi:10.1016/j.jbiomech.2010.06.010

Eby, S.F., Song, P., Chen, S., Chen, Q., Greenleaf, J.F., An, K.-N., 2013. Validation of shear wave elastography in skeletal muscle. J. Biomech. 46, 2381–2387. doi:10.1016/j.jbiomech.2013.07.033

Eng, C.M., Pancheri, F.Q., Lieberman, D.E., Biewener, A.A., Dorfmann, L., 2014. Directional Differences in the Biaxial Material Properties of Fascia Lata and the Implications for Fascia Function. Ann. Biomed. Eng. 42, 1224–1237. doi:10.1007/s10439-014-0999-3

Englund, E.K., Elder, C.P., Xu, Q., Ding, Z., Damon, B.M., 2011. Combined diffusion and strain tensor MRI reveals a heterogeneous, planar pattern of strain development during isometric muscle contraction. AJP Regul. Integr. Comp. Physiol. 300, R1079–R1090. doi:10.1152/ajpregu.00474.2010

Fan, Y., Litven, J., Pai, D.K., 2014. Active volumetric musculoskeletal systems. ACM Trans. Graph. TOG 33, 152.

Fernandez, J.W., Hunter, P.J., 2005. An anatomically based patient-specific finite element model of patella articulation: towards a diagnostic tool. Biomech. Model. Mechanobiol. 4, 20–38. doi:10.1007/s10237-005-0072-0

Fernandez, J.W., Schmid, H., Hunter, P.J., 2006. A Framework for Soft Tissue and Musculo-skeletal Modelling: Clinical Uses and Future Challenges, in: Mechanics of Biological Tissue. Springer, pp. 339–354.
Findley, T.W., Shalwala, M., 2013. Fascia Research Congress Evidence from the 100 year perspective of Andrew Taylor Still. J. Bodyw. Mov. Ther. 17, 356–364. doi:10.1016/j.jbmt.2013.05.015
Fiorentino, N.M., Blemker, S.S., 2014. Musculotendon variability influences tissue strains experienced by the biceps femoris long head muscle during high-speed running. J. Biomech. 47, 3325–3333. doi:10.1016/j.jbiomech.2014.08.010
Fregly, B.J., Besier, T.F., Lloyd, D.G., Delp, S.L., Banks, S.A., Pandy, M.G., D'Lima, D.D., 2012. Grand challenge competition to predict in vivo knee loads. J. Orthop. Res. 30, 503–513. doi:10.1002/jor.22023
Hahn, D., Seiberl, W., Schwirtz, A., 2007. Force enhancement during and following muscle stretch of maximal voluntarily activated human quadriceps femoris. Eur. J. Appl. Physiol. 100, 701–709. doi:10.1007/s00421-007-0462-3
Hedenstierna, S., Halldin, P., Siegmund, G.P., 2009. Neck muscle load distribution in lateral, frontal, and rear-end impacts: a three-dimensional finite element analysis. Spine 34, 2626–2633.
Heidlauf, T., Klotz, T., Rode, C., Altan, E., Bleiler, C., Siebert, T., Röhrle, O., 2016. A multi-scale continuum model of skeletal muscle mechanics predicting force enhancement based on actin–titin interaction. Biomech. Model. Mechanobiol. 1–15. doi:10.1007/s10237-016-0772-7
Herzog, W., 2004. History dependence of skeletal muscle force production: Implications for movement control. Hum. Mov. Sci. 23, 591–604. doi:10.1016/j.humov.2004.10.003
Herzog, W., Leonard, T.R., 2005. The role of passive structures in force enhancement of skeletal muscles following active stretch. J. Biomech. 38, 409–415. doi:10.1016/j.jbiomech.2004.05.001
Herzog, W., Leonard, T.R., Joumaa, V., Mehta, A., 2008. Mysteries of muscle contraction. J. Appl. Biomech. 24, 1–13.
Hodgson, J.A., Chi, S.-W., Yang, J.P., Chen, J.-S., Edgerton, V.R., Sinha, S., 2012. Finite element modeling of passive material influence on the deformation and force output of skeletal muscle. J. Mech. Behav. Biomed. Mater. 9, 163–183. doi:10.1016/j.jmbbm.2012.01.010
Howley, S., 2014. Développement et approche de personnalisation d'un modèle numérique musculaire déformable du cou. Lyon 1.
Huijing, P.A., Yaman, A., Ozturk, C., Yucesoy, C.A., 2011. Effects of knee joint angle on global and local strains within human triceps surae muscle: MRI analysis indicating in vivo myofascial force transmission between synergistic muscles. Surg. Radiol. Anat. 33, 869–879. doi:10.1007/s00276-011-0863-1
Huijing, P., Baan, G.C., Rebel, G.T., 1998. Non-myotendinous force transmission in rat extensor digitorum longus muscle. J. Exp. Biol. 201, 683–691.
Inouye, J., Handsfield, G., Blemker, S., 2015. Fiber tractography for finite-element modeling of transversely isotropic biological tissues of arbitrary shape using computational fluid dynamics, in: Proceedings of the Conference on Summer Computer Simulation. Society for Computer Simulation International, pp. 1–6.
Kim, T., James, D.L., 2012. Physics-based character skinning using multidomain subspace deformations. Vis. Comput. Graph. IEEE Trans. On 18, 1228–1240.
Klein Horsman, M.D., Koopman, H.F.J.M., van der Helm, F.C.T., Prosé, L.P., Veeger, H.E.J., 2007. Morphological muscle and joint parameters for musculoskeletal modelling of the lower extremity. Clin. Biomech. 22, 239–247. doi:10.1016/j.clinbiomech.2006.10.003
Kockova, H., Cimrman, R., 2009. Implementation of skeletal muscle model with advanced activation control.
Kohout, J., Clapworthy, G.J., Zhao, Y., Tao, Y., Gonzalez-Garcia, G., Dong, F., Wei, H., Kohoutova, E., 2013. Patient-specific fibre-based models of muscle wrapping. Interface Focus 3, 20120062–20120062. doi:10.1098/rsfs.2012.0062

Kwah, L.K., Pinto, R.Z., Diong, J., Herbert, R.D., 2013. Reliability and validity of ultrasound measurements of muscle fascicle length and pennation in humans: a systematic review. J. Appl. Physiol. 114, 761–769. doi:10.1152/japplphysiol.01430.2011

Lee, D., 2011. Modeling and Simulation of Skeletal Muscle for Computer Graphics: A Survey. Found. Trends® Comput. Graph. Vis. 7, 229–276. doi:10.1561/0600000036

Lee, D., Li, Z., Sohail, Q.Z., Jackson, K., Fiume, E., Agur, A., 2015. A three-dimensional approach to pennation angle estimation for human skeletal muscle. Comput. Methods Biomech. Biomed. Engin. 18, 1474–1484. doi:10.1080/10255842.2014.917294

Lee, S.-H., Sifakis, E., Terzopoulos, D., 2009. Comprehensive biomechanical modeling and simulation of the upper body. ACM Trans. Graph. TOG 28, 99.

Levin, D.I.W., Gilles, B., Mädler, B., Pai, D.K., 2011. Extracting skeletal muscle fiber fields from noisy diffusion tensor data. Med. Image Anal. 15, 340–353. doi:10.1016/j.media.2011.01.005

Li, D., Sueda, S., Neog, D.R., Pai, D.K., 2013. Thin skin elastodynamics. ACM Trans. Graph. TOG 32, 49.

Maas, H., Baan, G.C., Huijing, P.A., 2001. Intermuscular interaction via myofascial force transmission: effects of tibialis anterior and extensor hallucis longus length on force transmission from rat extensor digitorum longus muscle. J. Biomech. 34, 927–940.

Moissenet, F., Chèze, L., Dumas, R., 2014. A 3D lower limb musculoskeletal model for simultaneous estimation of musculo-tendon, joint contact, ligament and bone forces during gait. J. Biomech. 47, 50–58. doi:10.1016/j.jbiomech.2013.10.015

Monti, R.J., Roy, R.R., Hodgson, J.A., Edgerton, V.R., 1999. Transmission of forces within mammalian skeletal muscles. J. Biomech. 32, 371–380.

Murai, A., Endo, Y., Tada, M., 2016. Anatomographic Volumetric Skin-Musculoskeletal Model and Its Kinematic Deformation With Surface-Based SSD. IEEE Robot. Autom. Lett. 1, 1103–1109. doi:10.1109/LRA.2016.2524069

Muramatsu, T., Muraoka, T., Kawakami, Y., Fukunaga, T., 2002. Superficial aponeurosis of human gastrocnemius is elongated during contraction: implications for modeling muscle-tendon unit. J. Biomech. 35, 217–223.

Pancheri, F.Q., Eng, C.M., Lieberman, D.E., Biewener, A.A., Dorfmann, L., 2014. A constitutive description of the anisotropic response of the fascia lata. J. Mech. Behav. Biomed. Mater. 30, 306–323. doi:10.1016/j.jmbbm.2013.12.002

Pappas, G.P., Asakawa, D.S., Delp, S.L., Zajac, F.E., Drace, J.E., 2002. Nonuniform shortening in the biceps brachii during elbow flexion. J. Appl. Physiol. 92, 2381–2389. doi:10.1152/japplphysiol.00843.2001

Purslow, P.P., 2010. Muscle fascia and force transmission. J. Bodyw. Mov. Ther. 14, 411–417. doi:10.1016/j.jbmt.2010.01.005

Ramaswamy, K.S., Palmer, M.L., van der Meulen, J.H., Renoux, A., Kostrominova, T.Y., Michele, D.E., Faulkner, J.A., 2011. Lateral transmission of force is impaired in skeletal muscles of dystrophic mice and very old rats: Lateral transmission of force in skeletal muscles of mice and rats. J. Physiol. 589, 1195–1208. doi:10.1113/jphysiol.2010.201921

Rana, M., Hamarneh, G., Wakeling, J.M., 2013. 3D fascicle orientations in triceps surae. J. Appl. Physiol. 115, 116–125. doi:10.1152/japplphysiol.01090.2012

Rehorn, M.R., Blemker, S.S., 2010. The effects of aponeurosis geometry on strain injury susceptibility explored with a 3D muscle model. J. Biomech. 43, 2574–2581. doi:10.1016/j.jbiomech.2010.05.011

Röhrle, O., Davidson, J.B., Pullan, A.J., 2012. A Physiologically Based, Multi-Scale Model of Skeletal Muscle Structure and Function. Front. Physiol. 3. doi:10.3389/fphys.2012.00358

Roux, A., Laporte, S., Lecompte, J., Gras, L.-L., Iordanoff, I., 2016. Influence of muscle-tendon complex geometrical parameters on modeling passive stretch behavior with the Discrete Element Method. J. Biomech. 49, 252–258. doi:10.1016/j.jbiomech.2015.12.006

Sachdeva, P., Sueda, S., Bradley, S., Fain, M., Pai, D.K., 2015. Biomechanical simulation and control of hands and tendinous systems. ACM Trans. Graph. TOG 34, 42.

Sanchez, C.A., Lloyd, J.E., Fels, S., Abolmaesumi, P., 2014. Embedding digitized fibre fields in finite element models of muscles. Comput. Methods Biomech. Biomed. Eng. Imaging Vis. 2, 223–236. doi:10.1080/21681163.2013.862861

Schenk, P., Siebert, T., Hiepe, P., Güllmar, D., Reichenbach, J.R., Wick, C., Blickhan, R., Böl, M., 2013. Determination of three-dimensional muscle architectures: validation of the DTI-based fiber tractography method by manual digitization. J. Anat. 223, 61–68. doi:10.1111/joa.12062

Schleip, R., Jäger, H., Klingler, W., 2012. What is "fascia"? A review of different nomenclatures. J. Bodyw. Mov. Ther. 16, 496–502. doi:10.1016/j.jbmt.2012.08.001

Scott, S.H., Loeb, G.E., 1995. Mechanical properties of aponeurosis and tendon of the cat soleus muscle during whole-muscle isometric contractions. J. Morphol. 224, 73–86. doi:10.1002/jmor.1052240109

Seiberl, W., Hahn, D., Kreuzpointner, F., Schwirtz, A., Gastmann, U., 2010. Force enhancement of quadriceps femoris in vivo and its dependence on stretch-induced muscle architectural changes. J. Appl. Biomech. 26, 256–264.

Siebert, T., Leichsenring, K., Rode, C., Wick, C., Stutzig, N., Schubert, H., Blickhan, R., Böl, M., 2015. Three-Dimensional Muscle Architecture and Comprehensive Dynamic Properties of Rabbit Gastrocnemius, Plantaris and Soleus: Input for Simulation Studies. PLoS ONE 10, e0130985. doi:10.1371/journal.pone.0130985

Siebert, T., Rode, C., Herzog, W., Till, O., Blickhan, R., 2008. Nonlinearities make a difference: comparison of two common Hill-type models with real muscle. Biol. Cybern. 98, 133–143. doi:10.1007/s00422-007-0197-6

Siebert, T., Rode, C., Till, O., Stutzig, N., Blickhan, R., 2016. Force reduction induced by unidirectional transversal muscle loading is independent of local pressure. J. Biomech. doi:10.1016/j.jbiomech.2016.02.053

Siebert, T., Till, O., Stutzig, N., Günther, M., Blickhan, R., 2014. Muscle force depends on the amount of transversal muscle loading. J. Biomech. 47, 1822–1828. doi:10.1016/j.jbiomech.2014.03.029

Sifakis, E.D., 2007. Algorithmic aspects of the simulation and control of computer generated human anatomy models.

Sifakis, E., Shinar, T., Irving, G., Fedkiw, R., 2007. Hybrid simulation of deformable solids, in: Proceedings of the 2007 ACM SIGGRAPH/Eurographics Symposium on Computer Animation. Eurographics Association, pp. 81–90.

Sinha, U., Malis, V., Csapo, R., Moghadasi, A., Kinugasa, R., Sinha, S., 2015. Age-related differences in strain rate tensor of the medial gastrocnemius muscle during passive plantarflexion and active isometric contraction using velocity encoded MR imaging: Potential index of lateral force transmission: Strain Rate Mapping of Calf Muscle Fibers. Magn. Reson. Med. 73, 1852–1863. doi:10.1002/mrm.25312

Si, W., Lee, S.-H., Sifakis, E., Terzopoulos, D., 2014. Realistic biomechanical simulation and control of human swimming. ACM Trans. Graph. TOG 34, 10.

Stecco, C., Macchi, V., Porzionato, A., Duparc, F., De Caro, R., 2011. The fascia: the forgotten structure. Ital. J. Anat. Embryol. 116, 127.

Stecco, C., Porzionato, A., Lancerotto, L., Stecco, A., Macchi, V., Ann Day, J., De Caro, R., 2008. Histological study of the deep fasciae of the limbs. J. Bodyw. Mov. Ther. 12, 225–230. doi:10.1016/j.jbmt.2008.04.041

Stelletta, J., Dumas, R., Lafon, Y., 2013. Effect of the muscle activation level distribution on normal stress field: a numerical study. Comput. Methods Biomech. Biomed. Engin. 16 Suppl 1, 164–166. doi:10.1080/10255842.2013.815951

Sturmat, M., Weichert, C., Siebert, T., Böl, M., 2012. A numerical validation approach of a finite element muscle model using optical data. PAMM 12, 127–128. doi:10.1002/pamm.201210054

Teran, J., Sifakis, E., Blemker, S.S., Ng-Thow-Hing, V., Lau, C., Fedkiw, R., 2005. Creating and simulating skeletal muscle from the visible human data set. Vis. Comput. Graph. IEEE Trans. On 11, 317–328.

Tilp, M., Steib, S., Schappacher-Tilp, G., Herzog, W., 2011. Changes in fascicle lengths and pennation angles do not contribute to residual force enhancement/depression in voluntary contractions. J. Appl. Biomech. 27, 64–73.

Turrina, A., Martínez-González, M.A., Stecco, C., 2013. The muscular force transmission system: Role of the intramuscular connective tissue. J. Bodyw. Mov. Ther. 17, 95–102. doi:10.1016/j.jbmt.2012.06.001

Van Loocke, M., Lyons, C.G., Simms, C.K., 2008. Viscoelastic properties of passive skeletal muscle in compression: Stress-relaxation behaviour and constitutive modelling. J. Biomech. 41, 1555–1566. doi:10.1016/j.jbiomech.2008.02.007

Van Loocke, M., Lyons, C.G., Simms, C.K., 2006. A validated model of passive muscle in compression. J. Biomech. 39, 2999–3009. doi:10.1016/j.jbiomech.2005.10.016

Webb, J.D., Blemker, S.S., Delp, S.L., 2014. 3D finite element models of shoulder muscles for computing lines of actions and moment arms. Comput. Methods Biomech. Biomed. Engin. 17, 829–837. doi:10.1080/10255842.2012.719605

Winters, T.M., Sepulveda, G.S., Cottler, P.S., Kaufman, K.R., Lieber, R.L., Ward, S.R., 2009. Correlation between isometric force and intramuscular pressure in rabbit tibialis anterior muscle with an intact anterior compartment. Muscle Nerve 40, 79–85. doi:10.1002/mus.21298

Wisdom, K.M., Delp, S.L., Kuhl, E., 2015. Use it or lose it: multiscale skeletal muscle adaptation to mechanical stimuli. Biomech. Model. Mechanobiol. 14, 195–215. doi:10.1007/s10237-014-0607-3

Wong, J., Kuhl, E., 2014. Generating fibre orientation maps in human heart models using Poisson interpolation. Comput. Methods Biomech. Biomed. Engin. 17, 1217–1226. doi:10.1080/10255842.2012.739167

Yucesoy, C.A., 2010. Epimuscular myofascial force transmission implies novel principles for muscular mechanics. Exerc. Sport Sci. Rev. 38, 128–134.

Yucesoy, C.A., Baan, G., Huijing, P.A., 2010. Epimuscular myofascial force transmission occurs in the rat between the deep flexor muscles and their antagonistic muscles. J. Electromyogr. Kinesiol. 20, 118–126. doi:10.1016/j.jelekin.2008.09.012

Zajac, F.E., 1988. Muscle and tendon: properties, models, scaling, and application to biomechanics and motor control. Crit. Rev. Biomed. Eng. 17, 359–411.

Zhang, C., Gao, Y., 2014. Effects of aging on the lateral transmission of force in rat skeletal muscle. J. Biomech. 47, 944–948. doi:10.1016/j.jbiomech.2014.01.026

Zhang, Y., Jordan, J.M., 2010. Epidemiology of Osteoarthritis. Clin. Geriatr. Med. 26, 355–369. doi:10.1016/j.cger.2010.03.001

Zhong, X., Epstein, F.H., Spottiswoode, B.S., Helm, P.A., Blemker, S.S., 2008. Imaging two-dimensional displacements and strains in skeletal muscle during joint motion by cine DENSE MR. J. Biomech. 41, 532–540. doi:10.1016/j.jbiomech.2007.10.026

Zhukov, L., Barr, A.H., 2003. Heart-muscle fiber reconstruction from diffusion tensor MRI, in: Proceedings of the 14th IEEE Visualization 2003 (VIS'03). IEEE Computer Society, p. 79.

Zöllner, A.M., Abilez, O.J., Böl, M., Kuhl, E., 2012. Stretching Skeletal Muscle: Chronic Muscle Lengthening through Sarcomerogenesis. PLoS ONE 7, e45661. doi:10.1371/journal.pone.0045661

Figure and table captions.

Figure 2.1: Origins and insertions of the thigh's muscles

Figure 2.2: Cross sections of the thigh's muscles, according to Figure 1

Figure 2.3: multi-body rigid model of the lower limb, with the equivalent mechanisms for the joints (left) and the muscle lines of action (right). From Moissenet et al. (2014).

Figure 2.4: meshing the muscles: (1) generic block of hexahedron with four parameters to define the number of elements per dimension, (2) generic block fitted on the reconstructed boundary of the muscle - the edges in red were reinforced with the thermomechanical beams used for the fiber modelling, (3) 3D solid mesh of the muscle, (4) quasi-rigid elements used to link the muscle to the bone – insertions on the muscle in red, on the bone in green.

Figure 2.5: Deformable model of the lower limb, (1) with a focus on the thigh, (2) on the knee with the modeling of the ligaments, the patella and the tendon, (3) on the vastus medialis with the fiber beams in red embedded in the muscle solid matrix.

Figure 2.6: For both the Heel Strike (HS) and the Loading Response (LR) steps, total forces (passive plus active parts) computed for each muscle of the musculoskeletal model, for the multi-body rigid model and the Finite Element (FE) model with the two configurations (without and with contacts between muscles). Note that some muscles did not produced forces and so were did not reported in this table. Abbreviations: gluteus maximus, medius, minimus (G_max, G_med, G_min); adductor longus, brevis, magnus (A_long, A_brev, A_mag); pectineus (Pect); gracilis (Grac); sartorius (Sart); semimembranosus (S_memb); semitendinosus (S_tend); biceps femoris long head, short head (BF_long, BF_short); rectus femoris (RF); vastus medialis, intermedialis, lateralis (V_med, V_int, V_lat)

Figure 2.7: Geometry of the muscle models after the simulation of the Loading Response step (1); representation of the sliced muscles for the model without contact (2) and with contact (3) two cross sections c1 and c2 (1). Abbreviations were provided with the previous figure.

Figure 2.1.

cf. attached file

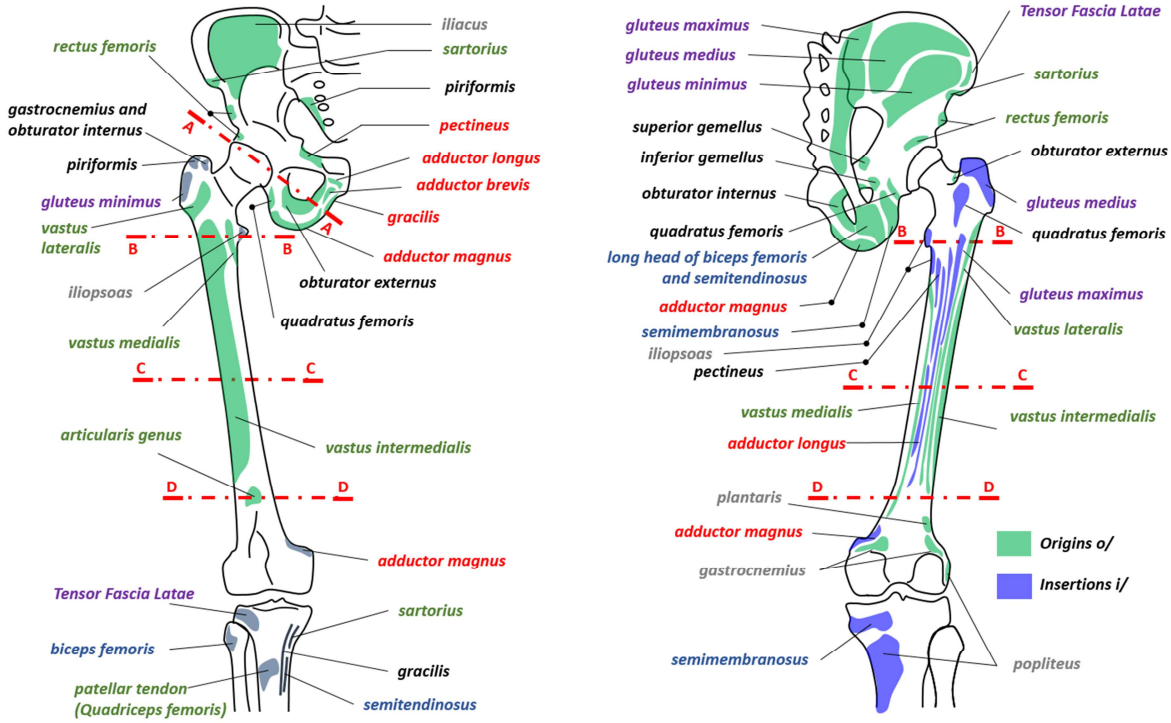

Figure 2.2.

cf. attached file

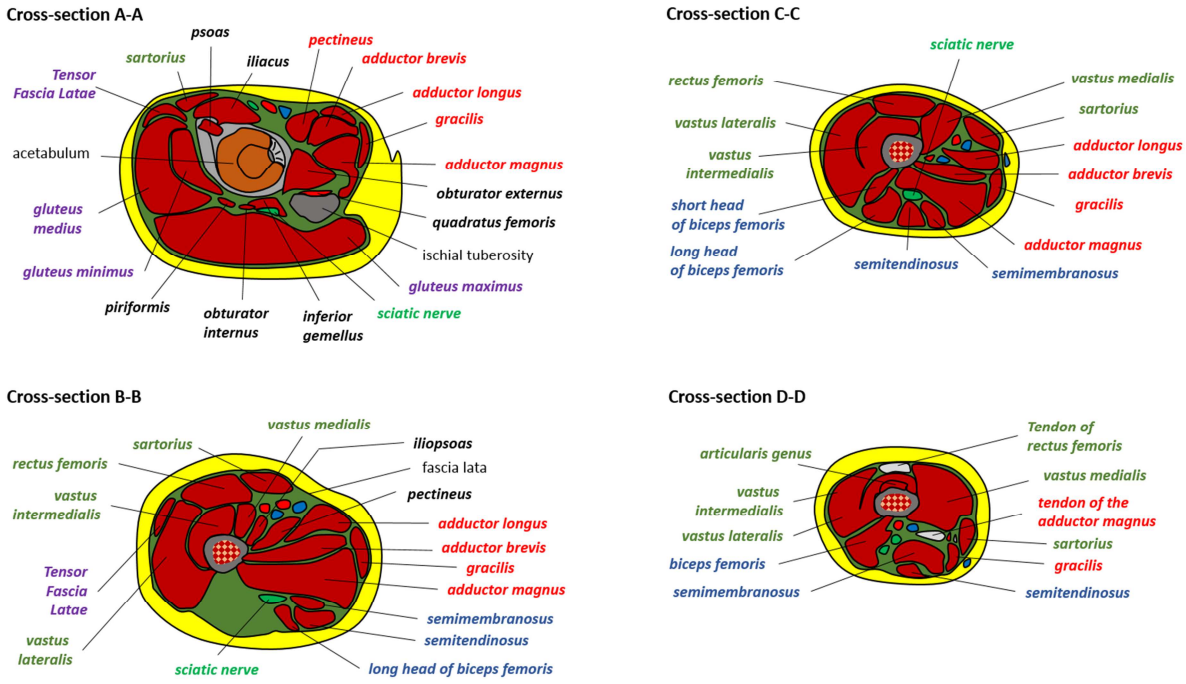

Figure 2.3.

cf. attached file

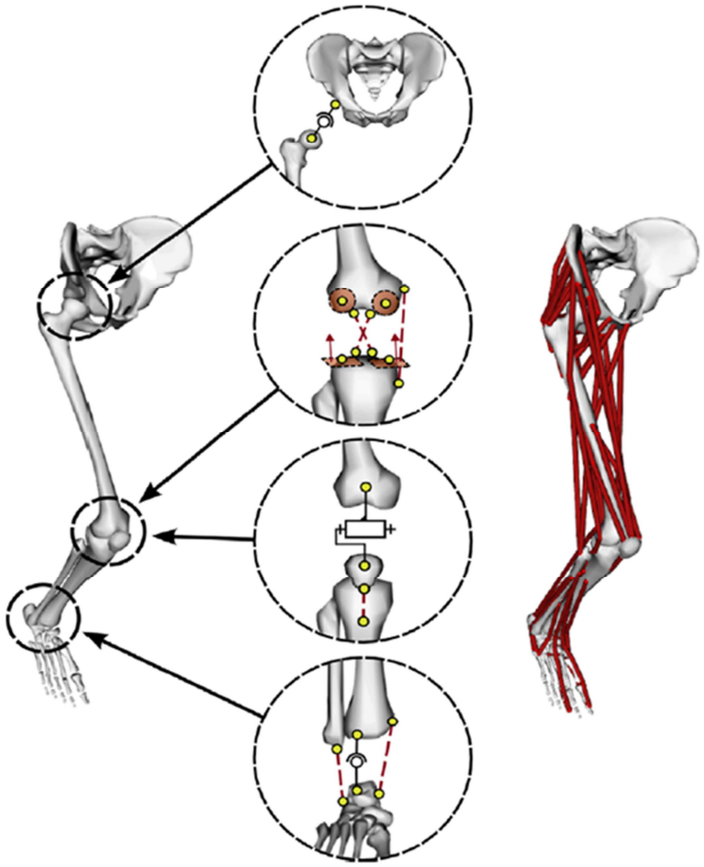

Figure 2.4.

cf. attached file

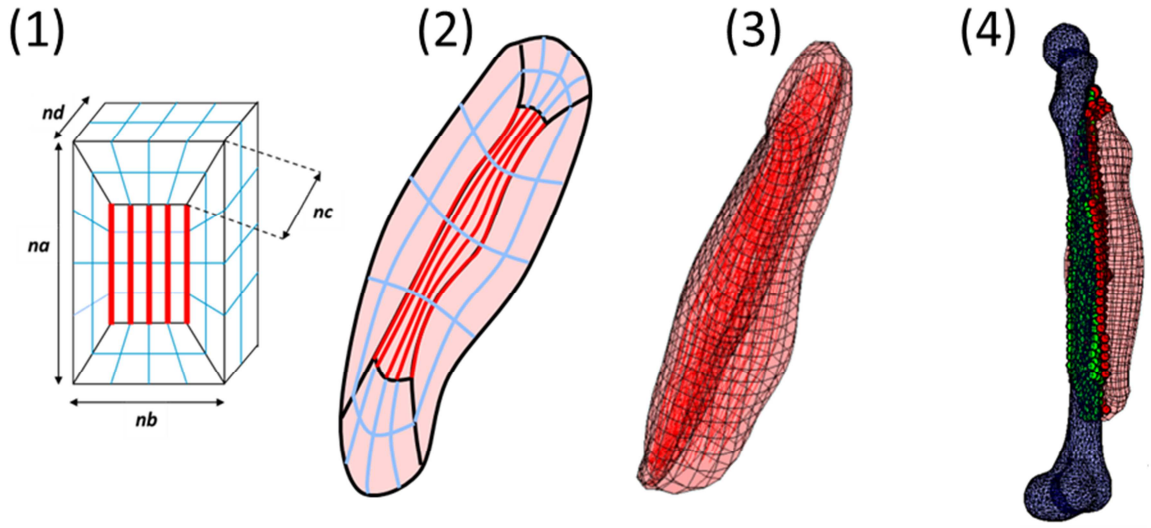

Figure 2.5.

cf. attached file

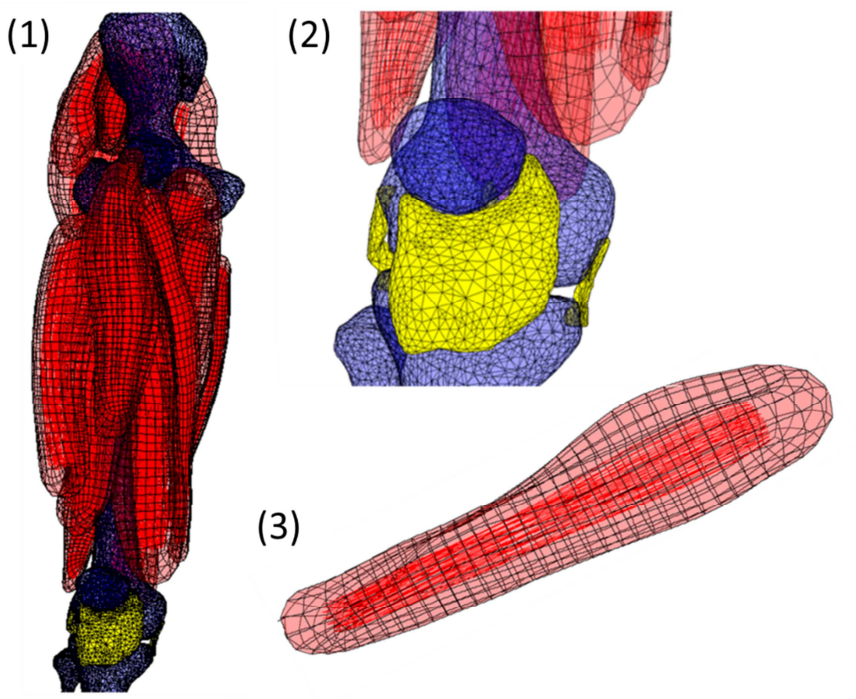

Table 2.6.

cf. attached file

Muscles	Total forces produced by muscles (N)		
	Multi-Body Rigid Model	FE Solid Model	
		Config 1 (w/o contact)	Config 2 (w/ contacts)
V_med	35	16	25
V_int	33	33	30
V_lat	34	34	36
Sart	319	307	324
RF	345	348	344
Pect	44	49	48
A_long	17	18	17
S_tend	187	187	187
BF_short	109	111	111
G_min	17	17	17

Heel Strike

Muscles	Total forces produced by muscles (N)		
	Multi-Body Rigid Model	FE Solid Model	
		Config 1 (w/o contact)	Config 2 (w/ contacts)
V_med	127	107	102
V_int	122	138	125
V_lat	122	122	122
Sart	37	31	29
RF	107	112	105
S_memb	62	38	63
G_max	369	368	370
G_med	673	655	677
G_min	559	532	447

Loading Response

Figure 2.7.

cf. attached file